# Intrinsic interfacial van der Waals monolayers and their effect on the high-temperature superconductor FeSe/$SrTiO_3$

Hunter Sims,[1,2,*] Donovan N. Leonard,[2] Axiel Yaël Birenbaum,[2] Zhuozhi Ge,[3] Tom Berlijn,[4,5] Lian Li,[3] Valentino R. Cooper,[2] Matthew F. Chisholm,[2] and Sokrates T. Pantelides[1,2]

[1]*Department of Physics and Astronomy, Vanderbilt University, Nashville, Tennessee 37235, USA*
[2]*Materials Science and Technology Division, Oak Ridge National Laboratory, Oak Ridge, Tennessee 37831, USA*
[3]*Department of Physics and Astronomy, West Virginia University, Morgantown, West Virginia 26506, USA*
[4]*Center for Nanophase Materials Sciences, Oak Ridge National Laboratory, Oak Ridge, Tennessee 37831, USA*
[5]*Computational Sciences and Engineering Division, Oak Ridge National Laboratory, Oak Ridge, Tennessee 37831, USA*

(Received 2 May 2018; revised manuscript received 27 May 2019; published 14 October 2019)

The sensitive dependence of monolayer materials on their environment often gives rise to unexpected properties. It was recently demonstrated that monolayer FeSe on a $SrTiO_3$ substrate exhibits a much higher superconducting critical temperature $T_c$ than the bulk material. Here, we examine the interfacial structure of FeSe/$SrTiO_3$ and the effect of an interfacial $Ti_{1+x}O_2$ layer on the increased $T_c$ using a combination of scanning transmission electron microscopy and density functional theory. We find $Ti_{1+x}O_2$ forms its own quasi-two-dimensional layer, bonding to both the substrate and the FeSe film by van der Waals interactions. The excess Ti in this layer can reconstruct the FeSe Fermi surface in a manner consistent with experimental observations. Moreover, the interfacial layer introduces symmetry-breaking distortions in the FeSe film that may favor a $T_c$ increase. These results suggest that this common substrate may be functionalized to modify the electronic structure of a variety of thin films and monolayers.

DOI: 10.1103/PhysRevB.100.144103

## I. INTRODUCTION

In his Nobel lecture, Kroemer opened with the statement "Often, it may be said that the interface is the device" [1]. Nowhere is this more true than in two-dimensional materials. The band gap of graphene provides an apt example. It is on the order of $\mu$eV in the freestanding material [2], arising from spin-orbit coupling, but reaches tens of meV on Cu(111) or hexagonal BN [3] or hundreds of meV in bilayer graphene [4]. The environmental effects are not limited to the band gap. Interactions in a two-dimensional (2D) material exhibit a strong dependence on the dielectric environment in neighboring substrate or vacuum layers [5]. Perhaps the most surprising recent example of substrate dependence in a two-dimensional material is the recent discovery of an order-of-magnitude increase in superconducting transition temperature when a single layer of FeSe is grown on $SrTiO_3$ (STO) [6–9]. Similar results have been obtained on $BaTiO_3$ [10] and both anatase and rutile $TiO_2$ [11,12] substrates, but the effect is absent on $Bi_2Se_3$ [13] and on graphene [14], where $T_c$ instead decreases as the thickness decreases (as is more typical of superconducting thin films such as Pb [15]). Bulk FeSe, the limiting case of the intercalated iron-pnictide/iron-chalcogenide system, exhibits a $T_c$ of only about 8 K [16] (reaching 37 K under pressure [17]), but in FeSe/$SrTiO_3$, $T_c$ increases by roughly an order of magnitude to 60–80 K, with one report reaching above 100 K [18].

It is reasonable to conclude that this enhanced superconductivity is directly related to the interaction between the FeSe monolayer (ML) and the substrate. Theoretical investigations into the role of the substrate have focused on the coupling between electronic states in the FeSe film and phonons in $SrTiO_3$ [19–22] or on charge transfer or doping between the substrate and monolayer [21]. Huang and Hoffman noted, however, that the structure of the interface between FeSe and STO has not been definitively established [23]. Li *et al.* [24] reported scanning-transmission-electron-microscopy (STEM) $Z$-contrast images that reveal a pair of $TiO_x$ layers (double layer), similar to the previously reported double-layered reconstruction of the bare STO(001) surface [25,26]. At about the same time, Zou *et al.* [27] proposed that the $\sqrt{13} \times \sqrt{13}$ STO(001) surface reconstruction persists in an interfacial $TiO_x$ double layer. They noted that O vacancies can account for the observation that ML FeSe on STO lacks a $\Gamma$ hole pocket in the angularly resolved photoemission spectroscopy (ARPES) data [7,28] and supporting this claim with diffraction experiments. As in the work of Cao *et al.* [29], an oxygen vacancy concentration of 50% is invoked to explain the doping. However, these proposed double-layer interfacial structures do not fully match the features of the $Z$-contrast images of Ref. [24]. More specifically, they do not account for the large spacing that is evident between the proposed pair of $TiO_x$ layers in the STEM images contained therein. The precise atomic structure of the interfacial layer is a necessary component of any explanation of the emergent properties of FeSe/STO.

In this work, we determine the structure of the interface, including a $Ti_{1+x}O_2$ interlayer that is bonded to both the

*hunter.sims@fmarion.edu; Present address: Department of Physics and Engineering, Francis Marion University, Florence, SC 29502, USA.

 

substrate and the FeSe ML by van der Waals (vdW) interactions, accounting for the observed large separation between the interlayer and the substrate. Both $Ti_{1+x}O_2$ and FeSe are essentially two-dimensional monolayers floating above the substrate, making $SrTiO_3/Ti_{1+x}O_2$/FeSe a van der Waals heterostructure. We show that the interlayer can be best described as a $(\sqrt{2} \times \sqrt{2})R45^\circ$ $Ti_{1.5}O_2$ layer. We demonstrate that the excess Ti in the interlayer contributes to the vanishing of the Fermi surface at the zone center [7,28]. This change to the electronic structure is significant because changes caused by oxygen vacancies, which have been discussed extensively along with those of excess Fe/Se ratio [11,27,29–31], have been excluded as the primary source of doping [11]. The 50% excess Ti dopes electrons into the Γ hole pocket in the FeSe band structure, with the extent of the doping inversely proportional to the strength of the bonding between the $Ti_{1+x}O_2$ and FeSe layers. Further, we find that the interlayer breaks the in-plane symmetry of the Fe sublattice yielding short and long Fe-Fe bonds of the same order of magnitude as that in superconducting $Fe_{1.01}Se$. Finally, we show that a floating, van der Waals bonded $Ti_{1+x}O_2$ monolayer is not unique to FeSe/$SrTiO_3$. A similar $TiO_2$-like layer exists in bulk $Cs_xTi_{2-x/4}O_4$ [32]. Previous work on bronze-phase $VO_2$ grown on $SrTiO_3$ reports an extra titanium oxide layer at the interface [33], which we now show is the same as that between FeSe and STO.

## II. METHODS

### A. Experiment

Single-layer FeSe films were grown on $SrTiO_3$(001) substrates by molecular beam epitaxy (MBE) in an ultrahigh-vacuum system with a base pressure below $1.0 \times 10^{-10}$ Torr. Nb-doped STO(001) (0.05 wt.%) substrates were first annealed at 950 °C for 30 min to produce an atomically flat surface. Then FeSe films were grown with a 0.2 monolayer-per-minute rate under Se-rich conditions (Fe/Se: 1/10) where Fe flux was provided by electron beam evaporation and Se from a Knudsen cell. The FeSe films followed a layer-by-layer growth mode and were post annealed at ∼550 °C for 2–3 h to remove excess Se and reach a superconducting state.

Scanning tunneling microscopy and spectroscopy (STM/STS) measurements were conducted in an ultrahigh-vacuum system with a base pressure of $2.0 \times 10^{-11}$ Torr, which is directly connected to the MBE growth chamber. Electrochemically etched polycrystalline W tips, or mechanically sharpened Pt tips, were used for STM imaging at room temperature and liquid helium temperature with the bias voltage applied to the sample. Tunneling spectra were taken at 6 K with a lock-in amplifier (at bias modulation of 0.4 mV at 860 Hz).

A Hitachi NB5000 FIB/SEM was used to prepare electron transparent foils for STEM imaging. To protect the FeSe monolayers from ion beam damage during preparation, the sample was coated with layers of C and Au. Thinning to electron transparency begun with deposition of a 25-$\mu$m-long, 4-$\mu$m-wide, ∼500-nm-thick tungsten capping layer to reduce "curtaining" during the final focused ion beam (FIB) thinning of the specimen. A 40-kV focused beam of Ga ions, with a current of 19.5 nA, was used to mill material away down into the substrate to a depth of 4–5 $\mu$m. The FeSe/$SrTiO_3$ sample was lifted from the bulk and transferred to a Cu omniprobe half-grid. A series of milling steps were then used to reduce the thickness of the lamella until it was electron transparent (<100 nm). The thinning was started with a 40-kV, 3.36-nA beam and thinned the sample to 1 $\mu$m thick. For the final milling step, the beam parameters were changed to 20 kV, 0.11 nA and the sample was thinned to <100 nm thick. To minimize Ga implantation effects and amorphous material on the surface of the FIB thinned sample, a Fischione Nanomill was operated at 900 eV with a 130 pA Ar+ beam for ion milling of the sample at ±10° for 15 min each side.

High-angle annular dark field (HAADF) imaging of the FeSe/$SrTiO_3$ interface was performed at 200 kV with a Nion UltraSTEM 200 using an illumination half-angle of 30 mrad and an inner detector half-angle of 65 mrad. Image simulations were carried out using the same parameters within a multislice model [34] including the quantum excitation of phonon model [35], as implemented in the program $\mu$STEM [36].

### B. Computation

All density functional theory calculations were performed within the PBESOLgeneralized gradient approximation [37] using the Vienna *ab initio* simulation package (VASP) [38]. We use the projector augmented-wave (PAW) [39] pseudopotentials of Kresse and Joubert [40] and the van der Waals corrections of Tkatchenko and Scheffler [41]. We use the DFT + $U$ method of Liechtenstein *et al.* [42] with $U = 3$ eV for Ti and 1.5 eV for Fe, taking $J = 0.9$ eV in both cases. To improve the accuracy of our results, we included Sr 4$s$ and 4$p$ and Ti 3$s$ and 3$p$ semicore states as valence states. $U_{Ti}$ was chosen as a typical value for bulk systems (e.g., Ref. [43]), while $U_{Fe}$ was chosen to give a reasonable Fe-Se height. Although reduced dimensionality can affect these parameters, we emphasize that neither the interface properties nor the presence of the in-plane distortion depends on $U$. Relaxations were performed on a Γ-centered $4 \times 4 \times 1$ $k$-point mesh using a plane-wave cutoff of 600 eV. Final calculations on the converged structure used an $8 \times 8 \times 1$ $k$ mesh, which was sufficient to converge all reported quantities. Our simulation cell consisted of three layers of $SrTiO_3$ with both faces terminated in $TiO_2$, the $Ti_{1+x}O_2$ interlayer ($x = 0.5$), a single layer of FeSe, and about 18 Å of vacuum. Terminating the back surface at the SrO layer rather than $TiO_2$ did not alter the properties of the interface. Structural relaxations were constrained to the experimental in-plane STO lattice parameter ($a = 3.905$ Å) to reduce the effect of the limited thickness of the STO slab.

STO surface reconstruction depends sensitively on sample preparation methods (see Ref. [44] and additional references contained therein). It follows that the structure of the interfacial monolayer may also depend on the substrate-growth conditions. For example, the substrate in Ref. [27] was grown at atmospheric pressure and annealed under $O_2$, leading to a different predeposition STO surface than is observed in the present samples, which were grown under ultrahigh-vacuum conditions. Furthermore, the surface undergoes additional reconstruction during the FeSe-monolayer growth (see Fig. 5(b)). The focus of this work, therefore, is the determination of the structure of the interfacial layer in our

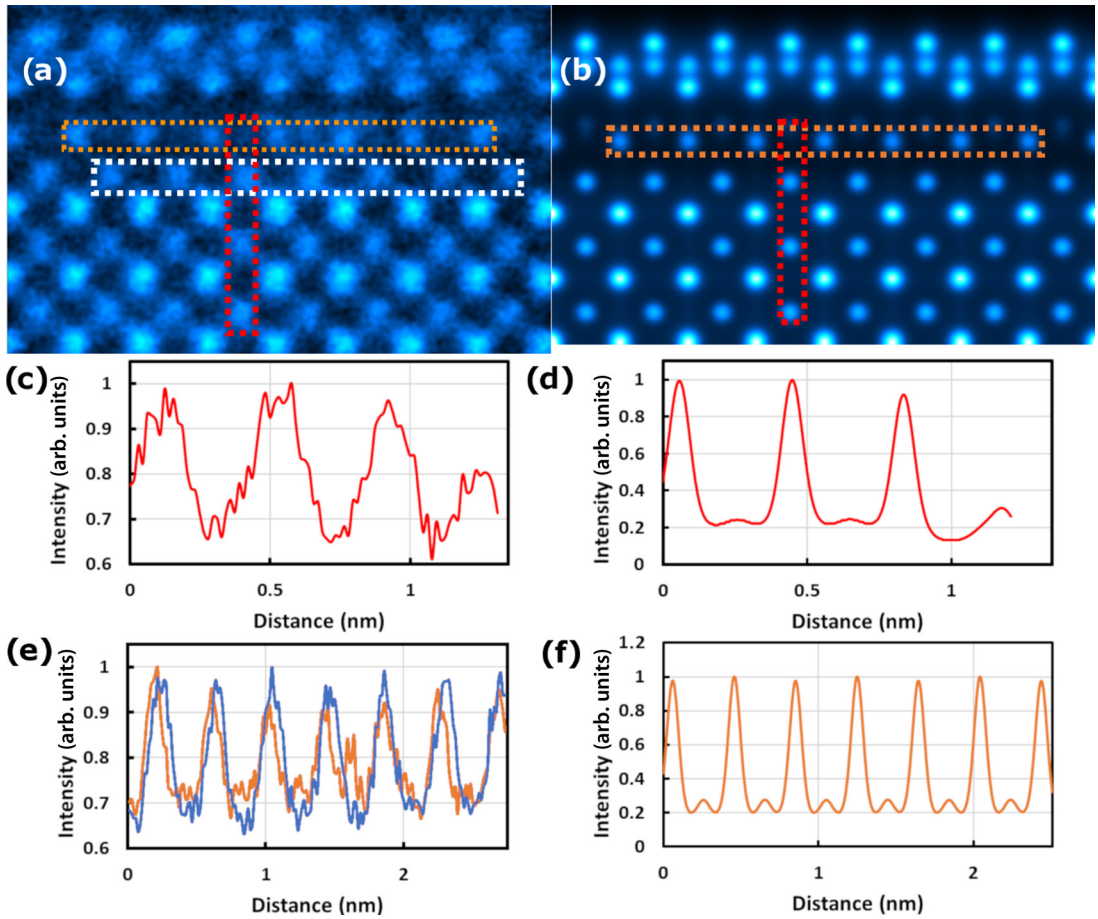


FIG. 1. (a) HAADF cross-sectional view of the FeSe/$SrTiO_3$ interface. An additional titanium oxide layer is visible above the standard $TiO_2$-terminated STO surface. (b) Simulated HAADF image using a multislice code [34], based on our interface structure (without capping layer). (c) Intensity profiles (averaged over a width of 8 pixels or about 13 pm) across the vertical (red) region of the interface layer and (d) the same region in the simulated image, both of which show clear indications of a faint atomic column between the bright Ti columns. (e) Intensity profile (with the same width) over the interfacial layer (orange) and $TiO_2$-terminated substrate (blue curve, white dashed rectangle), demonstrating that the additional intensity between the bright columns is again above the noise threshold, and (f) the same region in the simulated image, showing good agreement in all respects.

samples and investigation of its role in the superconducting properties of the FeSe monolayer.

## III. EXPERIMENTAL RESULTS

### A. STEM images and simulations

In Fig. 1(a) we present a $Z$-contrast aberration-corrected STEM image of the interface region captured at an acceleration voltage of 200 kV. See Appendix A for the STM/STS images obtained from the sample predeposition and postdeposition. The double titanium oxide termination is clearly visible, and one can discern faint features between the Ti columns in the second layer. These features become more apparent when viewing the intensity profile along vertical Ti columns [Fig. 1(c)] and along the $Ti_{1+x}O_2$ layer [Fig. 1(e)]. The height of the interfacial $Ti_{1+x}O_2$ layer (IL) above the normal $TiO_2$-terminated substrate is $2.55 \pm 0.20$ Å, which is itself $1.94 \pm 0.24$ Å above the SrO layer below. Both of these results are within the ranges reported by Li *et al.* [24]. The FeSe monolayer is $3.25 \pm 0.20$ Å above the IL. The STO IL distance represents more than a 30% increase in interlayer spacing compared to 1.95 Å in bulk STO. Comparison of this image and that of Ref. [24] with known reconstructions of the bare STO surface (see Appendix B) prompt us to seek a different atomic structure for this interfacial layer. Reference [24] attributes some of the additional features between the interfacial Ti columns to excess Se. Although both in this work and in Ref. [24] the samples were annealed so as to remove excess Se (as detailed in the Methods section), we nevertheless observe an additional atomic column between the brighter Ti columns [Fig. 1(a)]. Moreover, we note that Chen *et al.* [31] showed that excess Se is likely to be bound to substrate O vacancies. Although we cannot conclusively rule out the presence of excess Se in the second titanium oxide layer, we pursue an alternative origin for the signal between the bright Ti columns.

### B. Structural model

Guided by the HAADF images in this work and those in Ref. [24], we find the following constraints on a structural model for the interface. The alternating dark and bright

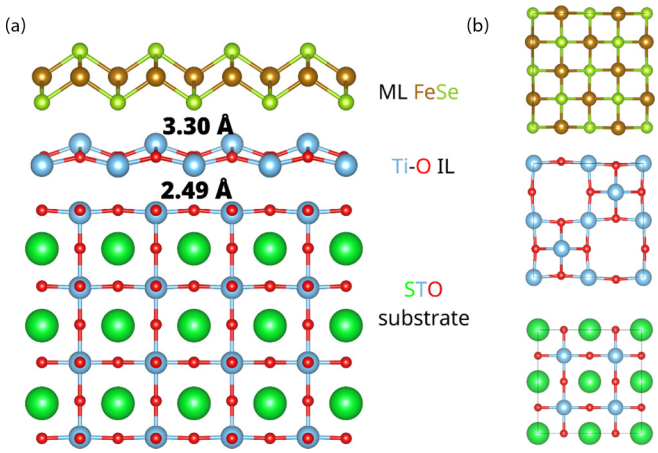


FIG. 2. Structure of the $FeSe/Ti_{1.5}O_2/SrTiO_3$ interface, projected along the [100] direction. (a) The interface with all atomic positions relaxed. The interlayer distances (2.49 and 3.30 Å) compare well with the experimental values ($2.55 \pm 0.20$ and $3.25 \pm 0.20$ Å) In addition to the increased distance between the substrate and the interfacial layer (2.49 Å compared to the expected 1.95 Å), we find that the terminal $TiO_2$ layer pulls closer to the layer below (1.82 Å). The extra Ti atoms in the interfacial layer are raised toward the FeSe film. (b) A top view of the three components of the interface: FeSe (top), $Ti_{1.5}O_2$ (middle), and $SrTiO_3$ (bottom).

features require that the symmetry of the IL is reduced compared to the STO substrate. The ubiquity of this feature leads to the conclusion that both in-plane directions possess this lowered symmetry. Although this can be accomplished with a $(\sqrt{2} \times \sqrt{2})R45^\circ$ reconstruction (as seen in the relaxed structure), we chose a $2 \times 2$ supercell to allow for additional distortions. The increased interlayer distance suggests that the IL must interrupt the expected Ti-O bonding pattern in the STO substrate, i.e., that the cations in the IL are not registered atop the underlying oxygen sublattice (and vice versa). Consequently, we have constructed an IL corresponding to a $(\frac{1}{2}, \frac{1}{2})$ shift of the normal $TiO_2$-terminated surface with additional Ti ions in half of the square cavities (as depicted in Fig. 2). The full-intensity Ti columns in the IL always sit above the Sr columns, and we enforce this constraint on both the *a*- and *b*-axis projections.

## IV. COMPUTATIONAL RESULTS AND DISCUSSION

We further refined our model using density functional theory, optimizing the full heterostructure with FeSe initialized in the checkerboard antiferromagnetic ordering and all other atomic species unpolarized. We find that it is necessary to introduce van der Waals corrections to prevent the interfacial layer from completely dissociating from the substrate. Applying the Tkatchenko-Scheffler method [41] yields an interlayer distance between the STO substrate and the IL of about 2.49 Å, in excellent agreement with the experimental value of $2.55 \pm 0.20$ Å (and compared to ~3 Å in the absence of vdW forces). We also find that the distance between the terminal $TiO_2$ layer and the SrO layer below is reduced to 1.82 Å (smaller than but within the error bars of our measurement), in agreement with Ref. [24]. See Fig. 2 for a detailed view of the calculated structure. The bottom of the FeSe layers sits about 3.3 Å above the IL.

To understand how the capping layer might affect the structure, we performed additional calculations with a FeTe layer on top of the FeSe ML (as is the case in the samples we imaged). Depending on the initial separation of the $Ti_{1.5}O_2$, FeSe, and FeTe layers, we found that we could relax structures with IL-FeSe distances of around 2.15 Å as well as 2.49 Å, with some additional distortion in the interface region in the former case. We therefore note that direct comparison of interlayer distance to superconducting properties must be made cautiously. All STM or ARPES experiments are performed *in situ* with a clean FeSe surface, while the STEM samples have been capped and have undergone further preparation. Further, Rooney *et al.* [45] found that the vdW gaps of monolayer selenides are particularly susceptible to discrepancies between experiment and DFT with vdW due to the presence of impurities or undulations at the interface.

A comparison of the HAADF images with our multislice STEM simulations [Fig. 1(b)] shows that the structure of our proposed interface agrees well with the experimental data. The agreement between the computed and observed structure leads us to conclude that we have accurately determined the FeSe/STO interface. The presence of the film causes the $Ti_{1.5}O_2$ layer to lift off from the STO substrate and form a separate interlayer that forms vdW assisted bonds to both substrate and film. Gao *et al.* [33] reported a titanium oxide layer between STO and monoclinic bronze-phase $VO_2$ that possesses similar properties. In Appendix C, we show a relaxed structure using the same methods employed in this study that gives good agreement with the experimental images. Notably, we find that in that system the IL bonds chemically with the deposited film while still forming vdW bonds with the substrate. Furthermore, layer-resolved electron energy-loss spectra at the interface are consistent with the change in coordination and/or nominal charge state found in our structure (a similar result is obtained by Li *et al.* in FeSe/STO [24]). Given that a floating $Ti_{1+x}O_2$ monolayer also appears between complex oxides with dissimilar symmetries, we hypothesize that such monolayers may provide an alternate path toward epitaxial heterointerfaces that lack a continuous perovskite lattice structure.

The present calculations show that the interlayer in the $FeSe/SrTiO_3$ system is not merely a passive glue holding substrate and film together. In fact, the interfacial Ti atoms develop magnetic moments of slightly less than $1\mu_B$ that we calculate to prefer a ferromagnetic orientation. Forcing a (necessarily frustrated) antiferromagnetic ordering in the IL yields an excited state about 1.5 meV/Ti higher in energy, suggesting that there may be competing magnetic states at finite temperature. Long-range magnetic order at the interface is likely to reduce $T_c$ and perhaps give rise to vortices, both of which contradict experiment. To explore other possibilities, we performed additional calculations under the constraint of no net spin. Relaxations yielded a similar atomic structure but a reduction of the IL-FeSe interlayer distance to about 2.5 Å. The distance between the IL and the STO substrate is increased to 2.8 Å (just outside the error bars of our measurement). As we emphasize below, both cases give rise to similar trends in the electronic structure of FeSe.

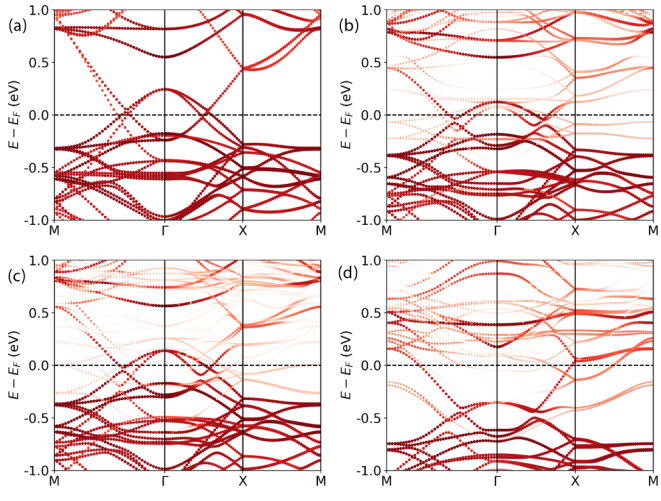


FIG. 3. Fe $d$ band structure of the (a) a free-standing FeSe monolayer, (b) a FeSe monolayer with a neighboring $Ti_{1.5}O_2$ layer (using the experimental interlayer distance), (c) full heterostructure with the same interlayer spacings, and (d) full heterostructure with the nonmagnetic interlayer spacings. Due to our $2 \times 2$ unit cell both the $M$ pockets are folded back to the Γ point. The addition of the interlayer in (b) nearly fills the hole pocket. Reintroducing the substrate reverses this trend somewhat (c). The nonmagnetic structure fully eliminates the hole pocket (d). The amount of hybrid Fe $d$/Se $p$ orbital character is indicated by the darkness of the red.

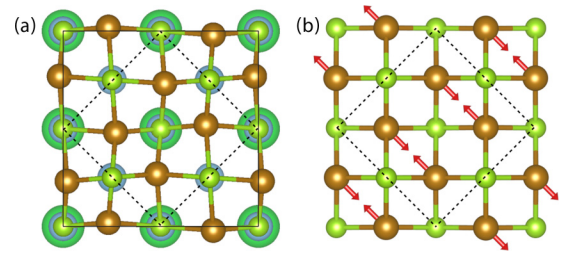


FIG. 4. View down the [001] direction of the $FeSe/Ti_{1+x}O_2/SrTiO_3$ interface, with the $(\sqrt{2} \times \sqrt{2})R45^\circ$ reconstruction indicated with dotted black lines. (a) Complete relaxed structure with Fe distortions exaggerated. One notes a distortion of the FeSe lattice such that neighboring diagonals are alternatingly closer or farther apart. In the magnetic (nonmagnetic) structure, for the diagonals along [110], the short distance is 2.75 Å (2.68 Å) and the long distance is 2.78 Å (2.82 Å). Along the perpendicular [1$\bar{1}$0] direction, these distances are 2.75 and 2.76 Å (2.72 and 2.80 Å), respectively. (b) An exaggerated schematic of the distortions between the [110] diagonals.

The position of the Γ hole pocket varies with the IL-FeSe distance. Figure 3 illustrates the effect of the IL and of the variation in interlayer spacing on the band structure (note that the bands are backfolded due to the larger unit cell, which means that the $M$ point in ARPES is now also at Γ). We plot the FeSe band structure of (a) bare ML FeSe, (b) ML FeSe with the $Ti_{1.5}O_2$ IL (with the observed interlayer spacing), (c) FeSe/magnetic IL/STO with the interlayer spacing observed in STEM, and (d) FeSe/nonmagnetic IL/STO with the larger interlayer spacing. All band structure calculations are computed in the nonmagnetic case, as is the common practice in Fe-based superconductors due to the inability of a static mean field method such as DFT to capture magnetic fluctuations [46–51]. In the IL/ML structure at the observed spacing [Fig. 3(b)], the hole pocket is nearly pushed below the Fermi level. In Fig. 3(c), the proximity of the STO substrate to the IL leaves the Γ pocket closer to the Fermi level than that of the bare ML [Fig. 3(a)] but higher than in Figs. 3(b) and 3(d). In Fig. 3(d), the Γ pocket is now well below the Fermi level. The trend from Fig. 3(c) to 3(d) can be explained by considering the distances between the IL and ML: A shorter distance reflects stronger bonding and thus a greater reconstruction of the bands. Reference [11] concludes that interfacial oxygen vacancies cannot be the primary mechanism for the doping of the FeSe monolayer grown on anatase $TiO_2$. Here, we have shown that excess Ti in this $Ti_{1.5}O_2$ interlayer promotes the filling of the hole pocket (to a degree that varies with interlayer spacing), an effect that is likely enhanced by oxygen vacancies.

McQueen *et al.* [52] observed that bulk $Fe_{1.01}Se$ undergoes a small orthorhombic distortion below 90 K such that two Fe-Fe distances emerge, differing by about 1.5 pm. We find that similar short and long Fe-Fe bond lengths arise from the interface structure (as seen in Fig. 4). These distortions are absent from the calculated structure when the FeSe monolayer is placed on the typical $TiO_2$-terminated STO substrate (i.e., without the interfacial layer). The $Ti_{1.5}O_2$ interlayer breaks the $C_4$ symmetry of the Fe sublattice, leaving only $C_2$ symmetry. Consequently, we find that the Fe atoms shift from their positions in the square lattice, forming alternating "long" and "short" distances differing in length by about 0.03 Å (0.2 Å) in the magnetic (nonmagnetic) structure. The size of the distortions arising from the magnetic structure is comparable to that seen in bulk $Fe_{1.01}Se$. Calculating the electron-phonon coupling proved infeasible in our 90-atom simulation cell. Recently, Coh and co-workers [53] showed that, although the epitaxial strain from STO stabilizes FeSe against shear distortions, the tendency toward such distortions enhances the coupling to certain FeSe phonon modes associated with the $M$ electron pocket. Using a modified semilocal potential and Eliashberg theory, they computed a $T_c$ of 20–25 K. In addition, it has been argued that the superconductivity in monolayer FeSe can be enhanced by a coupling between the Fe $d$ electrons and the phonons in the substrate that is peaked at small momenta [8,22,54]. Our resolved structure of the interface will allow for a better understanding of this mechanism.

## V. SUMMARY AND CONCLUSIONS

In summary, we have determined that the naturally occurring double titanium oxide surface reconstruction on STO(001) forms a $(\sqrt{2} \times \sqrt{2})R45^\circ$ $Ti_{1.5}O_2$ layer at the interface between $SrTiO_3$ and monolayer FeSe. This interfacial layer is bonded to both substrate and film by van der Waals forces. Our DFT + TS calculations show that this layer, which appears and facilitates epitaxy in at least one other complex oxide heterointerface, at least partially fills the Γ hole pocket as observed in ARPES measurements. This layer

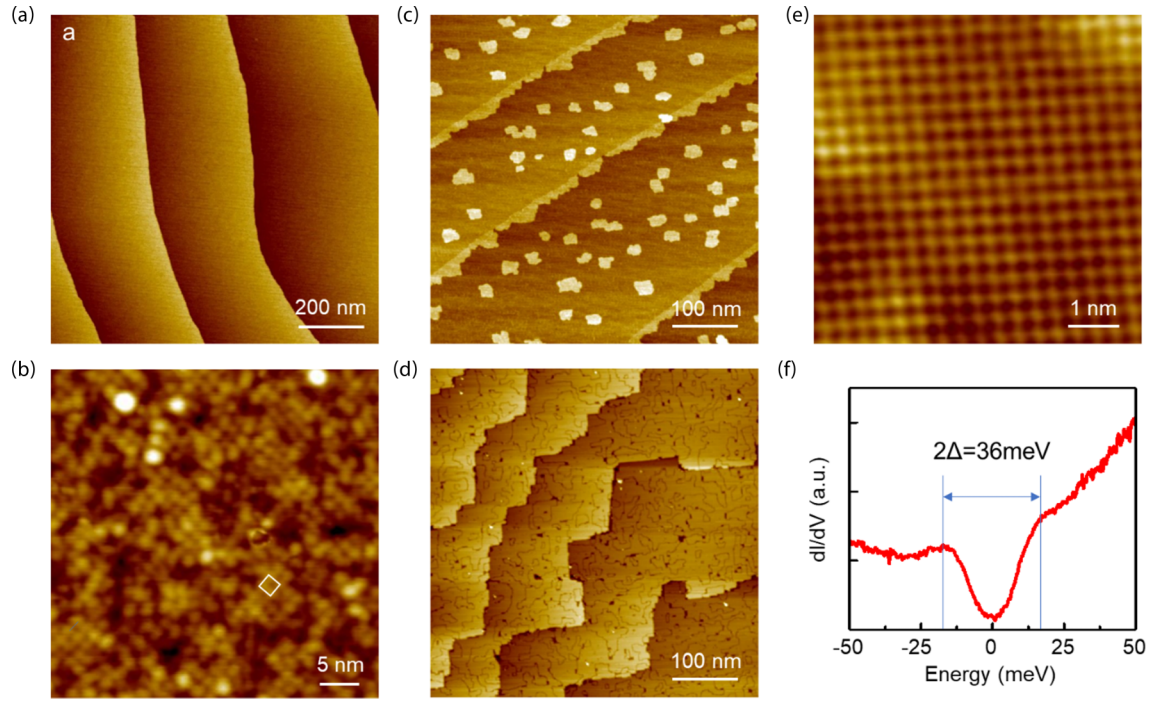


FIG. 5. (a) Large-scale STM image of a STO(001) substrate after annealing in UHV, showing a step-terrace morphology ($V_s = 1.3$ V, $I_t = 0.1$ nA). (b) Closeup view of the surface reveals mostly disordered structures. Nevertheless, partial ordering can be found including the $c(4 \times 4)$ structure, as outlined by a white box ($V_s = 2.0$ V, $I_t = 0.3$ nA). (c) STM image of an as-grown monolayer layer FeSe film on STO(001), where the film is conformal to the step-terrace morphology of the STO(001) substrate. Also observed are second-layer FeSe islands nucleated on top of the first layer, as well as along the step edges ($V_s = 1.0$ V, $I_t = 0.1$ nA). (d) STM image of monolayer FeSe/STO annealed at 550°C for up to 3 h to remove the excess Se ($V_s = -0.9$ V, $I_t = 0.1$ nA). (e) Atomic resolution STM image of FeSe showing a $(1 \times 1)$ square lattice with $a = 3.9$ Å, consistent with a monolayer FeSe strained to the in-plane STO(001) ($V_s = -50$ mV, $I_t = 0.3$ nA). (f) $dI/dV$ spectrum taken on the FeSe film at 6 K, indicating a superconducting gap of $\Delta = 18$ meV (half of the spacing between the coherence peaks).

also supports an in-plane distortion in the FeSe ML that scales inversely with the IL-FeSe interlayer distance. This van der Waals bonded interlayer is therefore essential for a full understanding of the superconducting properties of this system and should be included in future theories. Further theoretical and experimental investigation is required, particularly of the phonon properties of the IL, to fully elucidate the role of the $Ti_{1+x}O_{2-y}$ interlayer in the electronic and magnetic properties of FeSe and to see whether its effect can be replicated in other layered superconductors.

## ACKNOWLEDGMENTS

DFT calculations and related analysis were supported by U. S. DOE Grant No. DE-FG02-09ER46554 and the McMinn endowment at Vanderbilt University (H.S. and S.T.P.). They were performed at the National Energy Research Scientific Computing Center, a DOE Office of Science User Facility supported by the Office of Science of the U. S. Department of Energy under Contract No. DE-AC02-05CH11231. Work at ORNL is sponsored by the U. S. Department of Energy, Office of Science, Basic Energy Sciences, Materials Sciences and Engineering Division (D.N.L., A.Y.B., T.B., V.R.C., and M.F.C.). Work at West Virginia University (Z.G. and L.L.) is supported by the U. S. National Science Foundation, Division of Materials Research (Grant No. DMR-1335215). H.S. wishes to acknowledge helpful communication with G.-X. Zhang and A. Tkatchenko concerning the application of vdW-TS to PBESOL. We also wish to acknowledge useful conversations with T. A. Maier concerning the theory of superconductivity.

## APPENDIX A: STM/STS CHARACTERIZATION

Figure 5 contains STM and STS data obtained from our pregrowth subtrate [Figs. 5(a) and 5(b)], as-grown film [Fig. 5(c)], and post-anneal FeSe/STO [Figs. 5(d) and 5(e)]. We also present the $dI/dV$ spectrum collected at 6 K [Fig. 5(f)], showing a superconducting gap $\Delta = 18$ meV.

## APPENDIX B: IMAGE SIMULATIONS OF KNOWN STO SURFACE RECONSTRUCTIONS

In addition to the interface structure presented in this work, we considered other double titanium oxide layers based on STO surface reconstructions. In Fig. 6 we present $\mu$STEM simulations of the $(2 \times 1)$ STO surface reconstruction of Ref. [25]. Simulations of the $(4 \times 2)$ [55] and $\sqrt{13} \times \sqrt{13}$ [56] reconstructions are found in Figs. 7 and 8. Note that all simulated images are generated and presented using the same scale.

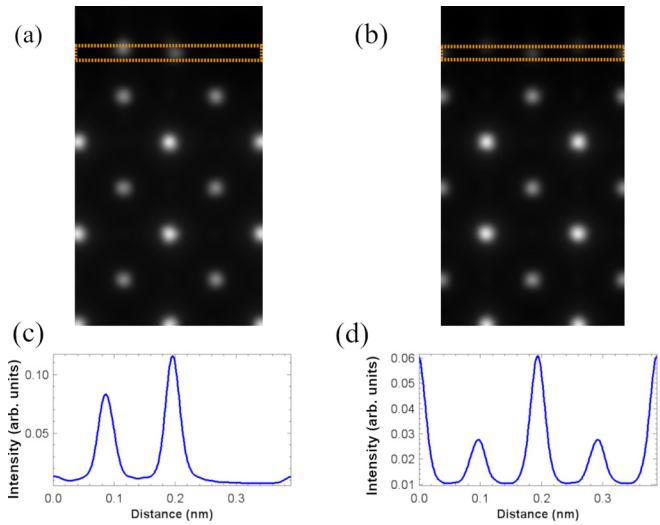


FIG. 6. Simulated HAADF images of the view down the *a* and *b* crystallographic directions of the $(2 \times 1)$ surface reconstruction of Ref. [25] [(a) and (b), respectively, with the corresponding line profiles appearing in (c) and (d)]. The view along *b* is roughly consistent with the full-/half-intensity pattern of the STEM images presented in the main text, although the partial-intensity columns are larger in magnitude than in our images (both real and simulated). However, the view along *a* does not agree with the experimental images (requiring an explanation for why only one orientation is observed); the full-intensity column appears over the Ti atoms and not the Sr atoms, meaning that the Ti-O bonding is not interrupted and there is no significant van der Waals assisted bonding and thus no increased interlayer distance.

## APPENDIX C: BRONZE-PHASE $VO_2$ ON $SrTiO_3$

While investigating the double titanium oxide layer in the FeSe/STO system, we became aware of another heterostructure with a similar interfacial structure. Gao *et al.* [33] reported epitaxial growth of bronze-phase $VO_2$ on STO despite the significant structural mismatch between the two materials. They presented HAADF images revealing the existence of an extra atomic layer between the $TiO_2$-terminated STO surface and the $VO_2$ film that closely resembles that in this work. We modeled this interface using the same $(\sqrt{2} \times \sqrt{2})$ IL as in FeSe/IL/STO and found that the pattern of Ti atoms in the IL closely matches the bottom O layer in $VO_2$(B). Relaxation of the structure yields a similar van der Waals assisted interface, albeit one with stronger bonding between the IL and film. The structural model of this interface can be seen in Fig. 9.

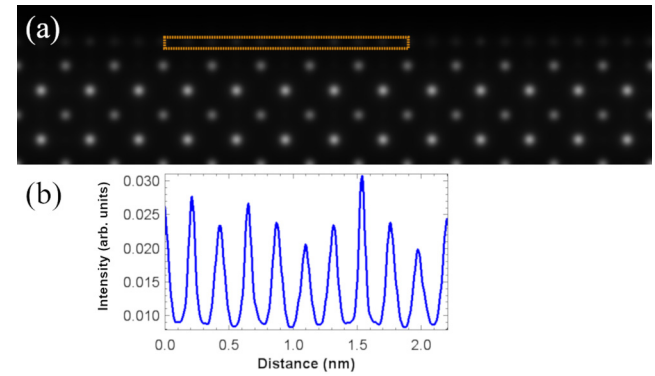


FIG. 8. (a) Simulated HAADF images of the $R33.7^\circ$ $(\sqrt{13} \times \sqrt{13})$ surface reconstruction of Ref. [56]. (b) Line profile across the second Ti-O layer. In this case, although there are similarities between the appearance of this layer and that seen experimentally in the FeSe/STO interface, neither the periodicity nor the magnitude of the Ti column intensities agree with the latter.

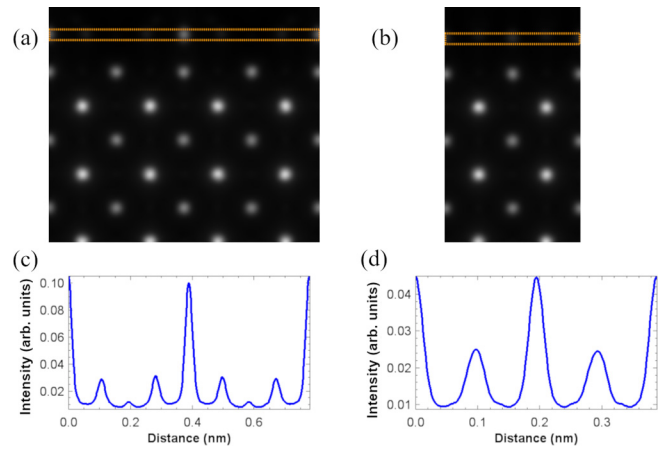


FIG. 7. Simulated HAADF images of the view down the *a* and *b* crystallographic directions of the $(4 \times 2)$ surface reconstruction of Ref. [55] [(a) and (b), respectively, with the corresponding line profiles appearing in (c) and (d)]. Again, the view along *b* agrees somewhat with the FeSe/STO interface, but the same caveats apply as in the $(2 \times 1)$ structure.

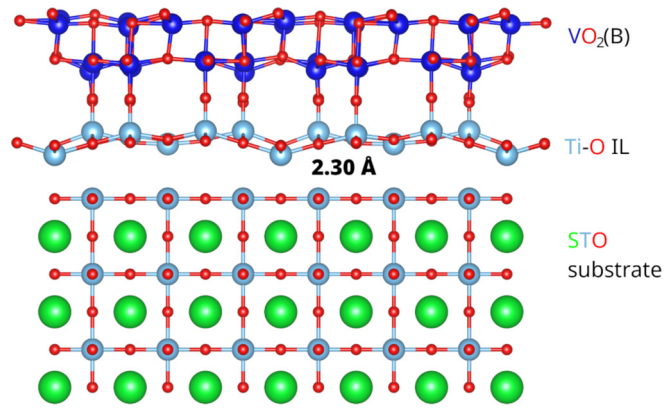


FIG. 9. Relaxed structure of the $VO_2$(B)/$Ti_{1+x}O_2$/$SrTiO_3$ interface, based on the experimental results of Ref. [33]. The buckling of the interfacial layer is more pronounced here, as the $Ti_{1.5}O_2$ layer partially conforms to the structure of the layer above. Unlike in FeSe/STO, the interfacial layer forms chemical bonds with $VO_2$, allowing the monoclinic bronze phase to grow epitaxially on cubic STO.

[1] H. Kroemer, Rev. Mod. Phys. **73**, 783 (2001).
[2] M. Gmitra, S. Konschuh, C. Ertler, C. Ambrosch-Draxl, and J. Fabian, Phys. Rev. B **80**, 235431 (2009).
[3] G. Giovannetti, P. A. Khomyakov, G. Brocks, P. J. Kelly, and J. van den Brink, Phys. Rev. B **76**, 073103 (2007).
[4] Y. Zhang, T.-T. Tang, C. Girit, Z. Hao, M. C. Martin, A. Zettl, M. F. Crommie, Y. R. Shen, and F. Wang, Nature (London) **459**, 820 (2009).
[5] D. Y. Qiu, F. H. da Jornada, and S. G. Louie, Phys. Rev. B **93**, 235435 (2016).
[6] W. Qing-Yan, L. Zhi, Z. Wen-Hao, Z. Zuo-Cheng, Z. Jin-Song, L. Wei, D. Hao, O. Yun-Bo, D. Peng, C. Kai, W. Jing, S. Can-Li, H. Ke, J. Jin-Feng, J. Shuai-Hua, W. Ya-Yu, W. Li-Li, C. Xi, M. Xu-Cun, and X. Qi-Kun, Chin. Phys. Lett. **29**, 037402 (2012).
[7] D. Liu, W. Zhang, D. Mou, J. He, Y.-B. Ou, Q.-Y. Wang, Z. Li, L. Wang, L. Zhao, S. He, Y. Peng, X. Liu, C. Chen, L. Yu, G. Liu, X. Dong, J. Zhang, C. Chen, Z. Xu, J. Hu *et al.*, Nat. Commun. **3**, 931 (2012).
[8] J. J. Lee, F. T. Schmitt, R. G. Moore, S. Johnston, Y.-T. Cui, W. Li, M. Yi, Z. K. Liu, M. Hashimoto, Y. Zhang, D. H. Lu, T. P. Devereaux, D.-H. Lee, and Z.-X. Shen, Nature (London) **515**, 245 (2014).
[9] P. Zhang, X.-L. Peng, T. Qian, P. Richard, X. Shi, J.-Z. Ma, B. B. Fu, Y.-L. Guo, Z. Q. Han, S. C. Wang, L. L. Wang, Q.-K. Xue, J. P. Hu, Y.-J. Sun, and H. Ding, Phys. Rev. B **94**, 104510 (2016).
[10] R. Peng, H. C. Xu, S. Y. Tan, H. Y. Cao, M. Xia, X. P. Shen, Z. C. Huang, C. H. P. Wen, Q. Song, T. Zhang, B. P. Xie, X. G. Gong, and D. L. Feng, Nat. Commun. **5**, 5044 (2014).
[11] H. Ding, Y.-F. Lv, K. Zhao, W.-L. Wang, L. Wang, C.-L. Song, X. Chen, X.-C. Ma, and Q.-K. Xue, Phys. Rev. Lett. **117**, 067001 (2016).
[12] S. N. Rebec, T. Jia, C. Zhang, M. Hashimoto, D.-H. Lu, R. G. Moore, and Z.-X. Shen, Phys. Rev. Lett. **118**, 067002 (2017).
[13] A. Eich, N. Rollfing, F. Arnold, C. Sanders, P. R. Ewen, M. Bianchi, M. Dendzik, M. Michiardi, J.-L. Mi, M. Bremholm, D. Wegner, P. Hofmann, and A. A. Khajetoorians, Phys. Rev. B **94**, 125437 (2016).
[14] C.-L. Song, Y.-L. Wang, Y.-P. Jiang, Z. Li, L. Wang, K. He, X. Chen, X.-C. Ma, and Q.-K. Xue, Phys. Rev. B **84**, 020503(R) (2011).
[15] M. M. Özer, J. R. Thompson, and H. H. Weitering, Nat. Phys. **2**, 173 (2006).
[16] F.-C. Hsu, J.-Y. Luo, K.-W. Yeh, T.-K. Chen, T.-W. Huang, P. M. Wu, Y.-C. Lee, Y.-L. Huang, Y.-Y. Chu, D.-C. Yan, and M.-K. Wu, Proc. Natl. Acad. Sci. USA **105**, 14262 (2008).
[17] S. Medvedev, T. M. McQueen, I. A. Troyan, T. Palasyuk, M. I. Eremets, R. J. Cava, S. Naghavi, F. Casper, V. Ksenofontov, G. Wortmann, and C. Felser, Nat. Mater. **8**, 630 (2009).
[18] J.-F. Ge, Z.-L. Liu, C. Liu, C.-L. Gao, D. Qian, Q.-K. Xue, Y. Liu, and J.-F. Jia, Nat. Mater. **14**, 285 (2015).
[19] B. Rosenstein, B. Y. Shapiro, I. Shapiro, and D. Li, Phys. Rev. B **94**, 024505 (2016).
[20] S. Zhang, J. Guan, X. Jia, B. Liu, W. Wang, F. Li, L. Wang, X. Ma, Q. Xue, J. Zhang, E. W. Plummer, X. Zhu, and J. Guo, Phys. Rev. B **94**, 081116(R) (2016).
[21] Y. Zhou and A. J. Millis, Phys. Rev. B **93**, 224506 (2016).
[22] L. Rademaker, Y. Wang, T. Berlijn, and S. Johnston, New J. Phys. **18**, 022001 (2016).
[23] D. Huang and J. E. Hoffman, Annu. Rev. Condens. Matter Phys. **8**, 311 (2017).
[24] F. Li, Q. Zhang, C. Tang, C. Liu, J. Shi, C. Nie, G. Zhou, Z. Li, Wenhao Zhang, C.-L. Song, K. He, S. Ji, S. Zhang, L. Gu, L. Wang, X.-C. Ma, and Q.-K. Xue, 2D Mater. **3**, 024002 (2016).
[25] N. Erdman, K. R. Poeppelmeier, M. Asta, O. Warschkow, D. E. Ellis, and L. D. Marks, Nature (London) **419**, 55 (2002).
[26] G. Zhu, G. Radtke, and G. A. Botton, Nature (London) **490**, 384 (2012).
[27] K. Zou, S. Mandal, S. D. Albright, R. Peng, Y. Pu, D. Kumah, C. Lau, G. H. Simon, O. E. Dagdeviren, X. He, I. Božović, U. D. Schwarz, E. I. Altman, D. Feng, F. J. Walker, S. Ismail-Beigi, and C. H. Ahn, Phys. Rev. B **93**, 180506(R) (2016).
[28] S. He, J. He, W. Zhang, L. Zhao, D. Liu, X. Liu, D. Mou, Y.-B. Ou, Q.-Y. Wang, Z. Li, L. Wang, Y. Peng, Y. Liu, C. Chen, L. Yu, G. Liu, X. Dong, J. Zhang, C. Chen, Z. Xu *et al.*, Nat. Mater. **12**, 605 (2013).
[29] H.-Y. Cao, S. Tan, H. Xiang, D. L. Feng, and X.-G. Gong, Phys. Rev. B **89**, 014501 (2014).
[30] K. V. Shanavas and D. J. Singh, Phys. Rev. B **92**, 035144 (2015).
[31] M. X. Chen, Z. Ge, Y. Y. Li, D. F. Agterberg, L. Li, and M. Weinert, Phys. Rev. B **94**, 245139 (2016).
[32] I. E. Grey, C. Li, I. C. Madsen, and J. A. Watts, J. Solid State Chem. **66**, 7 (1987).
[33] X. Gao, S. Lee, J. Nichols, T. L. Meyer, T. Z. Ward, M. F. Chisholm, and H. N. Lee, Sci. Rep. **6**, 38168 (2016).
[34] L. J. Allen, S. D. Findlay, M. P. Oxley, and C. J. Rossouw, Ultramicroscopy **96**, 47 (2003).
[35] B. D. Forbes, A. V. Martin, S. D. Findlay, A. J. D'Alfonso, and L. J. Allen, Phys. Rev. B **82**, 104103 (2010).
[36] L. J. Allen, A. J. D'Alfonso, and S. D. Findlay, Ultramicroscopy **151**, 11 (2015).
[37] J. P. Perdew, K. Burke, and M. Ernzerhof, Phys. Rev. Lett. **77**, 3865 (1996).
[38] G. Kresse and J. Furthmüller, Comput. Mater. Sci. **6**, 15 (1996).
[39] P. E. Blöchl, Phys. Rev. B **50**, 17953 (1994).
[40] G. Kresse and D. Joubert, Phys. Rev. B **59**, 1758 (1999).
[41] A. Tkatchenko and M. Scheffler, Phys. Rev. Lett. **102**, 073005 (2009).
[42] A. I. Liechtenstein, V. I. Anisimov, and J. Zaanen, Phys. Rev. B **52**, R5467(R) (1995).
[43] Z. Hu and H. Metiu, J. Phys. Chem. C **115**, 5481 (2011).
[44] S. Gerhold, Z. Wang, M. Schmid, and U. Diebold, Surf. Sci. **621**, L1 (2014).
[45] A. P. Rooney, A. Kozikov, A. N. Rudenko, E. Prestat, M. J. Hamer, F. Withers, Y. Cao, K. S. Novoselov, M. I. Katsnelson, R. Gorbachev, and S. J. Haigh, Nano Lett. **17**, 5222 (2017).
[46] A. Subedi, L. Zhang, D. J. Singh, and M. H. Du, Phys. Rev. B **78**, 134514 (2008).
[47] Y. Xia, D. Qian, L. Wray, D. Hsieh, G. F. Chen, J. L. Luo, N. L. Wang, and M. Z. Hasan, Phys. Rev. Lett. **103**, 037002 (2009).
[48] K. Nakayama, T. Sato, P. Richard, T. Kawahara, Y. Sekiba, T. Qian, G. F. Chen, J. L. Luo, N. L. Wang, H. Ding, and T. Takahashi, Phys. Rev. Lett. **105**, 197001 (2010).

[49] M. Yi, D. H. Lu, R. G. Moore, K. Kihou, C.-H. Lee, A. Iyo, H. Eisaki, T. Yoshida, A. Fujimori, and Z.-X. Shen, New J. Phys. **14**, 073019 (2012).

[50] W. Malaeb, T. Yoshida, A. Fujimori, M. Kubota, K. Ono, K. Kihou, P. M. Shirage, H. Kito, A. Iyo, H. Eisaki, Y. Nakajima, T. Tamegai, and R. Arita, J. Phys. Soc. Jpn. **78**, 123706 (2009).

[51] I. Nishi, M. Ishikado, S. Ideta, W. Malaeb, T. Yoshida, A. Fujimori, Y. Kotani, M. Kubota, K. Ono, M. Yi, D. H. Lu, R. Moore, Z.-X. Shen, A. Iyo, K. Kihou, H. Kito, H. Eisaki, S. Shamoto, and R. Arita, Phys. Rev. B **84**, 014504 (2011).

[52] T. M. McQueen, A. J. Williams, P. W. Stephens, J. Tao, Y. Zhu, V. Ksenofontov, F. Casper, C. Felser, and R. J. Cava, Phys. Rev. Lett. **103**, 057002 (2009).

[53] S. Coh, M. L. Cohen, and S. G. Louie, New J. Phys. **17**, 073027 (2015).

[54] D.-H. Lee, Chin. Phys. B **24**, 117405 (2015).

[55] N. Erdman, O. Warschkow, M. Asta, K. R. Poeppelmeier, D. E. Ellis, and L. D. Marks, J. Am. Chem. Soc. **125**, 10050 (2003).

[56] D. M. Kienzle, A. E. Becerra-Toledo, and L. D. Marks, Phys. Rev. Lett. **106**, 176102 (2011).